Available online at www.sciencedirect.com
ScienceDirect
International Journal of Heat and Fluid Flow 28 (2007) 922–931
International Journal of HEAT AND FLUID FLOW
www.elsevier.com/locate/ijhff

Turbine blade showerhead film cooling: Influence of hole angle and shaping

Yiping Lu, David Allison, Srinath V. Ekkad *

Mechanical Engineering, Department Louisiana State University, Baton Rouge, LA 70803, United States

Received 27 June 2006; received in revised form 9 January 2007; accepted 23 January 2007
Available online 13 March 2007

Abstract

Detailed film cooling measurements are presented on a turbine blade leading edge model with three rows of showerhead holes. Experiments are run at a mainstream Reynolds number of 19,500 based on cylindrical leading edge diameter. One row of holes is located on the stagnation line and the other two rows are located at 615° on either side of the stagnation line. The three rows have compound angle holes angled 90° in the flow direction, 30° along the spanwise direction, and the two holes on either side of the stagnation row have and additional angle of 0°, 30°, and 45° in the transverse direction. The effect of hole shaping of the 30° and 45° holes is also considered. Detailed heat transfer coefficient and film effectiveness measurements are obtained using a transient infrared thermography technique. The results are compared to determine the advantages of shaping the compound angle for rows of holes off stagnation row. Results show that, the additional compound angle in the transverse direction for the two rows adjacent to the stagnation row provide significantly higher film effectiveness than the typical leading edge holes with only two angles. Results also show that, the shaping of showerhead holes provides higher film effectiveness than just adding an additional compound angle in the transverse direction and significantly higher effectiveness than the baseline typical leading edge geometry. Heat transfer coefficients are higher as the spanwise angle for this study is larger than typical leading edge geometries with an angle of 30° compared to 20° for other studies.
© 2007 Elsevier Inc. All rights reserved.

Keywords: Turbine; Blade; Film cooling; Holes

1. Introduction

With increases in needs for global energy production, the modern gas turbine engines are focused on improving performance and efficiency. Higher turbine inlet temperatures increase the thermal efficiency of these engines resulting in a need for more effective cooling schemes. In practice, relatively cool air from the aft compressor stages is injected through holes in the walls of hollow turbine airfoils in an effort to isolate the metal surface from the hot mainstream. The highest thermal load occurs at the leading edge of the airfoil, and failure often occurs in this region due to burn off or loss of material. Film cooling is typically applied on the leading edge through an array of hole rows called the showerhead. Effective cooling of the leading edge region of the airfoil is extremely critical due to the presence of the highest thermal load in that region. The flow environment near the leading edge is extremely complex with a stagnation mainstream, strong pressure gradients and curvature, and interaction between multiple rows of film-cooling holes. With the addition of film cooling in regions of thin boundary layers, the interactions between mainstream and coolant jets become increasingly complex. Increases in film effectiveness in the leading edge will lead to significant benefits in life and efficiency of the turbine blade.

There have been several studies in the past two decades focused on the leading edge area of an airfoil with film cooling. Majority of the literature has been covered in the book by Han et al. (2000). There have been several studies on leading edge showerhead film cooling in the

* Corresponding author. Tel.: +1 225 578 5901; fax: +1 225 578 5924.
E-mail address: ekkad@me.lsu.edu (S.V. Ekkad).

0142-727X/$ - see front matter © 2007 Elsevier Inc. All rights reserved.
doi:10.1016/j.ijheatfluidflow.2007.01.002

Nomenclature

C_p	specific heat (kJ/kg K)	T_f	film temperature (K)
D	film hole diameter at inlet (m)	T_∞	mainstream temperature (K)
Δ	leading edge diameter (m)	T_u	free stream mean turbulence intensity (%)
DR	coolant to mainstream density ratio, ρ_c/ρ_∞	T_w	local wall temperature (K)
k	thermal conductivity of test section material	U_c	coolant velocity (m/s)
L	length of film hole (m)	U_∞	mainstream velocity (m/s)
M	blowing ratio $\rho_c U_c/\rho_\infty U_\infty$	X	streamwise distance along the test plate (m)
Re	free stream Reynolds number ($U_\infty d/\nu$)	α	thermal diffusivity of test section material
ρ_c	coolant density (kg/m^3)	β	shaped hole flare angle (°)
ρ_∞	mainstream density (kg/m^3)	η	film cooling effectiveness
T_c	coolant temperature (K)	ν	kinematic viscosity of mainstream (m^2/s)

past. Mick and Mayle (1988), Karni and Goldstein (1989), Mehendale and Han (1992), Ou et al. (1992), Salcudean et al. (1994), Ekkad et al. (1998), Funazaki et al. (1997), Cruse et al. (1997), Ou and Rivir (2001) experimentally studied the leading edge showerhead film cooling problem and provided fundamental results that has helped designers provide better protection for the high heat load region. Recently, York and Leylek (2002a,b) studied leading edge film cooling using CFD. They compared their predictions with experiments by Cruse et al. (1997). In all the above studies, the holes were angled in two directions, one along the spanwise direction and another orthogonal to the flow direction. These hole geometries ensure that the coolant will exit along the spanwise direction and get pushed away along the surface downstream. The hole geometry is good for the stagnation row. However, the rule of thumb does not apply for the rows on either side of stagnation region as holes can be angled in the transverse direction resulting in possibly improved coverage.

Hole shaping has extensive benefits and seems like a natural extension towards a more slotlike behavior in film hole rows (Bunker, 2005). Bunker (2005) provided an extensive literature survey of shaped hole technology and provided examples and showed benefits of this design. However, shaped holes have been used along the suction and pressure surfaces downstream of the leading edge and not on the leading edge as shown in Bunker, 2005. Mouzon et al. (2005) presented an experimental study on leading edge film cooling with different shaped hole configurations. They had five rows of holes places at stagnation, 620°, and 640°. They had laidback fan shaped holes with widened exits clearly indicating higher cooling performance. They indicated that laterally expanded holes did not perform as well as laid back fan shaped holes. There was one more recent study by Reiss and Bolcs (2000) on possible hole shaping on leading edge hole rows. The holes were laid-back shaped type holes. They however did not have the additional transverse shaped holes. The present study focuses on hole shaping the side rows of the showerhead array. Since hole shaping the typical baseline holes where the film flow is along the spanwise direction at the leading edge is not possible, hole shaping of holes with an additional transverse angle of 30° and 45° only is considered.

In the present study, a transient infrared thermography technique is used for obtaining both heat transfer coefficient and film effectiveness from a single test. The transient IR technique is based on the two-equation, single test proposed by Vedula and Metzger (1991) and was demonstrated successfully by Ekkad et al. (2004). In this test, two images with surface temperature distributions are captured at two different times during the transient test. The test is typical of a transient liquid crystal technique experiment wherein the test surface at ambient is suddenly exposed to a hot mainstream and cold coolant jet. The surface temperature response is captured by the IR camera at different time instants during the transient test. Both η and h distributions are investigated and presented, on the leading edge of a blunt body, for various blowing ratios for cylindrical compound angle holes.

2. Test facility

Fig. 1 shows the facility used for the present study. The test setup consists of a blower connected to a 12 kW heater that heats the air to a free-stream temperature of 50 °C. The air is then routed through a section with baffles to ensure adequate mixing of the hot air to obtain a uniform temperature across the cross-section. The presence of the baffles inadvertently contributed to the high free-stream turbulence in the mainstream. A thermocouple was traversed across the test section to check for uniformity of the inlet thermal field. The air is then passed through a 2-D 4:1 converging nozzle. The hot air is effectively sealed such that no air leaks into the test section and affects the initial temperature condition of the test surface. The open gate allows the flow into a test section made of ABS plastic and has a cross-section of 33-cm width and 8.89-cm height. The components upstream of the test section are covered with insulation to minimize the heating time. The coolant air is provided from a separate compressed air supply and is metered for flow measurement.

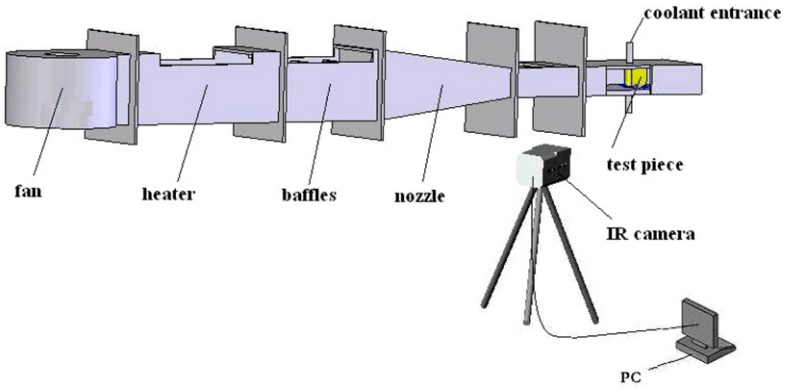

Fig. 1. Illustration of the test facility.

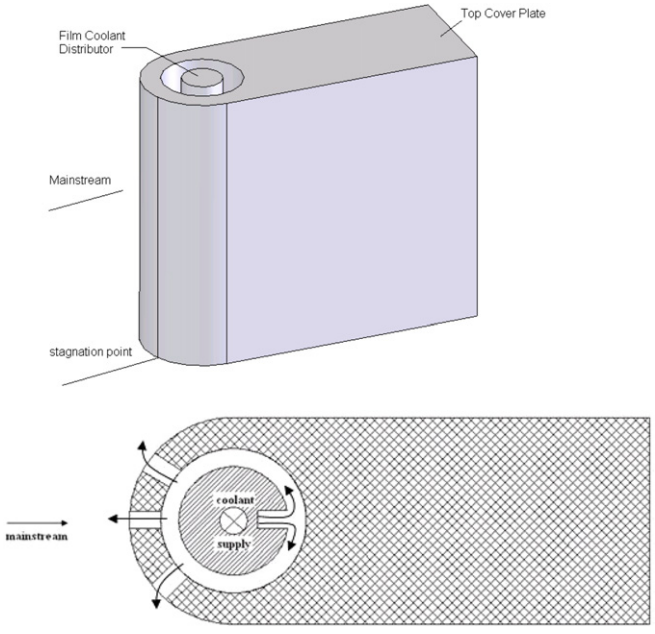

Fig. 2. Illustration of the test model.

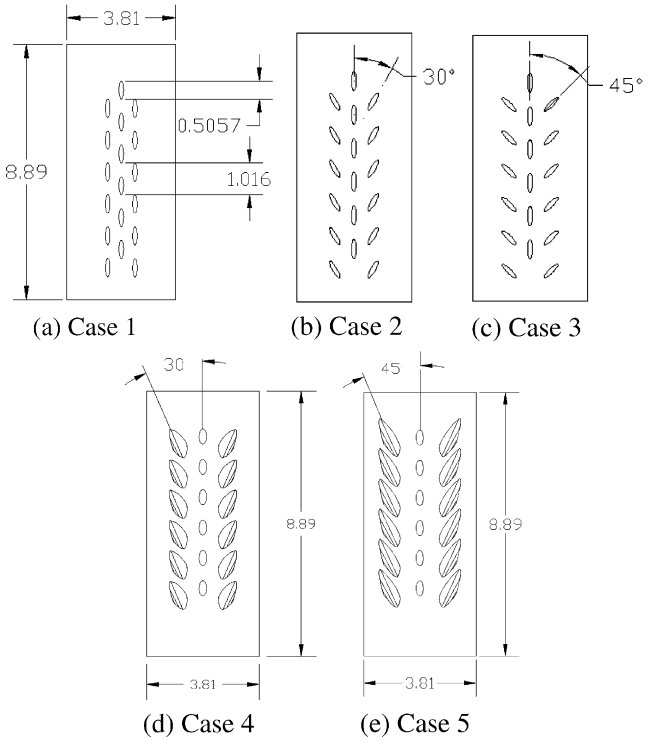

Fig. 3. Schematic of film holes arrangements (all dimensions in cm).

As seen in Fig. 2, the test model is a blunt body with a semi-cylinder leading edge and a flat after-body. For uniform approaching flow and turbulence, the leading edge of the test model was positioned at a distance of 33-cm downstream of the exit of the converging nozzle. The test model with ABS material ($\alpha = 7.157 * 10^{-8}\,\mathrm{m^2/s}$; $k = 0.15\,\mathrm{W/m\,K}$) in a 3D printing machine (Dimension™). The test model was 8.89-cm in height and the leading edge diameter was 3.81-cm. Film holes were located at stagnation line and ±15° from stagnation and spaced 4 film hole diameters in the spanwise direction. Each film hole was 0.254-cm diameter.

Fig. 3 shows the frontal views of the leading edge of the bluff body. The test surface had eighteen holes (3 rows of 6 holes each) and all film holes inclined 30° to the test surface in the spanwise direction and 90° to the flow direction. There were three cases considered here: the film hole inclined 0°, 30° and 45° to the test surface in the transverse direction, respectively. The hole to leading edge diameter ratio (D/Δ) is 0.067 and hole length to diameter ratio (L/D) at the stagnation row is 4.51 and longer for the rows adjacent to the stagnation. The shaped holes geometries are also shown. The shaped holes are designed based on defined geometries as shown in Fig. 4. In our study, the hole angle is compounded on the surface with 30° to the test surface in the spanwise direction and 90° to the flow direction and an additional 30° and 45° to the test surface in the transverse direction. The shaped-hole flare angle β is 5° in the present geometry.

The infrared thermography system used is a FLIR Systems ThermaCAM SC 500. The camera offers a high quality, non-intrusive method for obtaining thermal data through a commercially available software package for data analysis. The camera has a range of −40 °C to

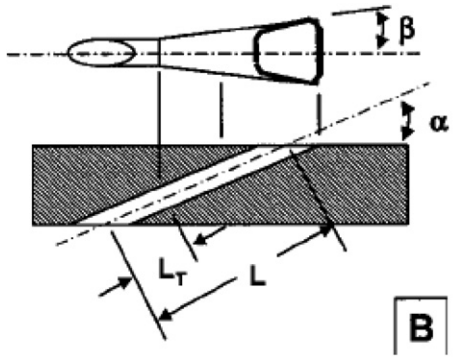

Fig. 4. Define shaped hole geometry (Bunker, 2005).

500 °C. The ThermaCAM 500 utilizes uncooled microbolometer longwave detectors to sense IR radiation. This makes it ideal for general thermal measurement applications. The SC 500 system features real time 14-bit digital output, a 320×240 pixel detector, precision temperature measurement, internal data storage, and outstanding thermal sensitivity. The camera has following specifications: the field of view and minimum focus distance are $24^0 \times 18^0$ and 0.5 m, respectively, the spectral range is 7.5–13 μm and accuracy is ±2% or 2 °C. The test surface is viewed through a stretched polyurethane sheet of thickness at 5 μm. The sheet is thin enough to cause very little effect on IR transmissivity. The system calibration is conducted using a thermocouple placed on the black painted test surface to act as the benchmark. This 36-gage thermocouple is used to estimate the emissivity of the test surface. The emissivity of the black painted test when viewed without the window is 0.96. The calibrated transmissivity for the polyurethane sheet was 0.75. Transmissivity and emissivity were checked over a range of temperatures from 25–50 °C. All calibration is in situ.

3. Procedure and analysis

The mainstream air is heated to approximately 50 °C and is bypassed away from the test section. When the bypass air temperature reaches the set temperature, the air is suddenly switched into the test section and the IR camera is triggered to take data at the same instant. The wall temperature monitored by the thermocouple used for emissivity estimation rises as the outside surface is heated during the transient test at a more gradual rate than mainstream temperature. The inside wall temperature is unaffected by the heating on the opposite side confirming the usage of the semi-infinite solid assumption under the test conditions. The test surface was modeled as a semi-infinite solid medium imposed by a sudden transient heating. The entire solid medium was initially at a uniform temperature before the transient test. During the transient heating test, each point on the surface will respond with different temperature at different time due to different heat transfer rate. Faster time of temperature change in response to the prescribed temperature during the transient test will produce higher heat transfer coefficient and vice verse. Typically the mainstream temperature increases from the initial temperature to about 90% of the set temperature in the first five seconds and then during the next 10–15 s reaches the maximum and then steadies. The coolant temperature is, however, maintained at the initial temperature.

Vedula and Metzger (1991) presented a method wherein two color change times can be obtained from a single transient test at every location. If during the transient, the liquid crystal coating indicates one surface temperature (T_{w1}) at time, t_1 and another surface temperature (T_{w2}) at time, t_2. Basically, two events are measured at every point leading to the solution of both h and T_f from the simultaneous solution of the two equations:

$$\frac{T_{w1}-T_i}{T_f-T_i} = 1-\exp\left(\frac{h_f^2\alpha t_1}{k^2}\right)erfc\left(\frac{h_f\sqrt{\alpha t_1}}{k}\right)$$
$$\frac{T_{w2}-T_i}{T_f-T_i} = 1-\exp\left(\frac{h_f^2\alpha t_2}{k^2}\right)erfc\left(\frac{h_f\sqrt{\alpha t_2}}{k}\right) \quad (6)$$

The wall temperatures are captured at set instants of time over the entire surface. Several events are recorded and stored and the wall temperatures at every surface location are obtained from the IR images. The camera however can provide images at 60 images/second but only selected events are stored for processing. Other events are used for visualization of the jet-mainstream interaction and also provide valuable understanding of the processed heat transfer results. The choice of selection of separate event times was based on the analysis of the validity of Duhamel's integration. The short times have high uncertainty and large times will create possible violation of the semi-infinite solid assumption. The two times should have far enough apart to satisfy the two extremes. Any other choices (20 and 50 s) or a regression analysis of the measured wall temperatures will also produce the same results. The mainstream temperature response is also measured and the inner wall temperature was also measured to ensure the application of semi-infinite wall assumption. The minimum thickness of the wall is where the coolant cavity is and is 0.635 cm which is reasonably sufficient for experimental test durations under 2 min. The two equations shown above are then solved simultaneously with the two known wall temperatures at the same locations and both unknowns h and η are determined. This has been demonstrated successfully by Ekkad et al. (2004) for a single hole injecting coolant on to a leading edge model.

Uncertainty in the calculation comes from measurement of initial, mainstream and coolant temperatures. Estimated uncertainty in initial and wall temperature (ΔT_i) is ±1.1 °C, mainstream temperature (ΔT_∞) is ±1.1 °C, and coolant temperature (ΔT_c) is ±1.1 °C. The camera frame rate is 60 Hz resulting in a time error of ±1.6% and the test surface property uncertainty is estimated at ±3%. The resulting average uncertainty using the methodology proposed by Kline and McClintock (1953) for heat transfer coeffi-

cient and film effectiveness is ±8.5% and ±11.2%, respectively. However, uncertainty for local film effectiveness depends on the local value. Uncertainty for effectiveness measurements is ±0.05.

4. Results and discussion

Tests were conducted in the low speed wind tunnel at a free-stream Reynolds number of 19,500 based in leading edge diameter (Δ) and incident mainstream velocity ($U_\infty = 9.2$ m/s). Free-stream streamwise turbulence intensity in the test duct was around 9% and the calculated integral length scale for turbulence was 1.09-cm. Heat transfer coefficient normalized as Frossling number ($Nu/Re^{0.5}$) and film effectiveness distributions are presented for three blowing ratios of 0.5, 1.0 and 1.5 and a coolant-to-mainstream density ratio of 1.0 (air).

4.1. Effect of blowing ratio

Fig. 5 shows the effect of blowing ratio on film effectiveness distributions for the baseline case (0°). Both detailed distributions (contour plots) and spanwise averaged (line plot) distributions are presented. The contour plots are displayed only for the region $0 < x/D < 10$ where the majority of the variations occur. Results show the high effectiveness immediately downstream of injection with two clear peaks downstream of the two rows of holes. The first peak occurs at stagnation as the coolant is injected along the span of the leading edge. The second peak also sees very little directional change due to the mainstream. Film effectiveness increases with increasing blowing ratio with a somewhat level off in increases as blowing ratio approaches 1.5. These results are consistent with results presented by Funazaki et al. (1997) with similar hole geometry.

Fig. 6 presents the effect of blowing ratio on Frossling number for the baseline (0°) case. Immediately downstream of the holes the Frossling numbers are greatly enhanced. The enhancement over an uncooled surface with the presence of high free-stream turbulence for this geometry will

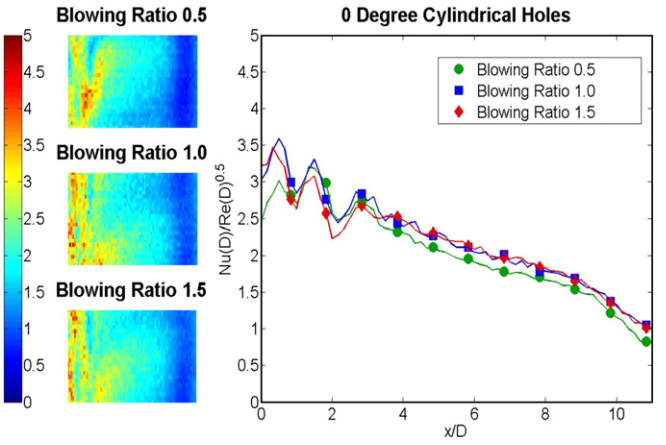

Fig. 6. Effect of blowing ratio on Frossling number distributions for Case 1.

be around 1.75–2.0 just downstream of the stagnation holes. The effect of blowing ratio is minimal compared to the overall increases caused by injection of film. These results are also consistent with previous studies on leading edge film cooling geometry. The present study just downstream of the hole shows higher Frossling numbers than previous studies Mouzon et al. (2005, 2000) primarily because of the different spanwise angle used for the present hole geometry. The spanwise angle in the present study is 30° compared to a shallow angle of 20° in the previous studies. This causes increased interaction between mainstream and coolant jets resulting in significantly higher Frossling numbers immediately downstream of injection than for the shallow angle case. The values immediately downstream are 3.0–3.5 for the present study whereas there are 2.0–2.75 for the shallow angle cases.

Fig. 7 presents the effect of blowing ratio on film effectiveness distributions for Case 2 (30°). The second peak of high effectiveness is farther downstream due to the compound angle and is significantly enhanced compared to the baseline case. The effect is even more significant at $M = 0.5$

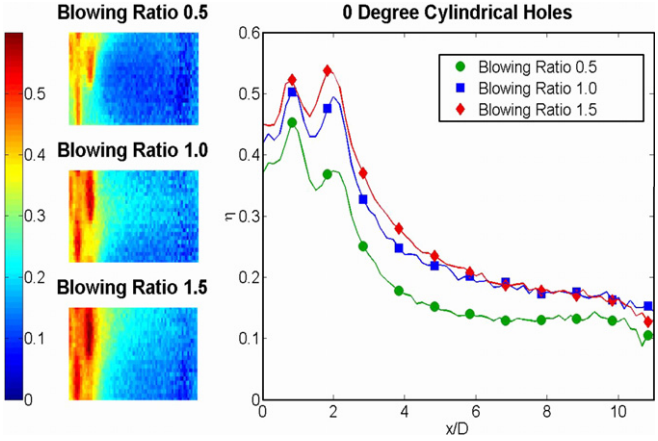

Fig. 5. Effect of blowing ratio on film effectiveness distributions for Case 1.

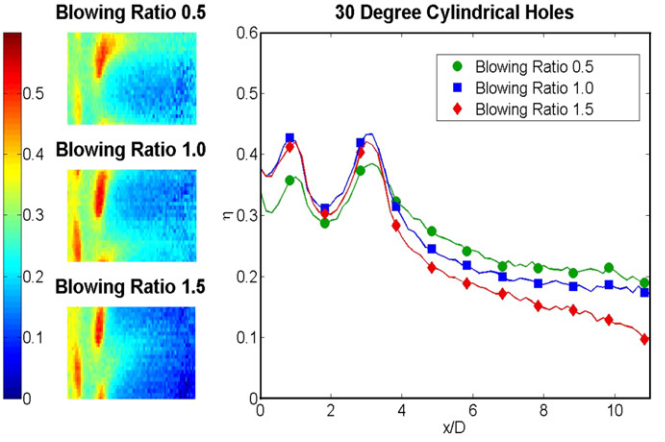

Fig. 7. Effect of blowing ratio on film effectiveness distributions for Case 2.

and 1.0 farther downstream of injection where the film effectiveness is around 0.2 compared to 0.1 for Case 1. With increasing blowing ratio up to 1.5, the drop-off is significant leading to a conclusion that jet lift-off may be enabled at higher blowing ratio with the additional compound angle.

Fig. 8 presents the effect of blowing ratio on Frossling number distributions for Case 2 (30°). The detailed distributions show immediate high enhancement downstream of injection. In this case, it appears that heat transfer is enhanced more for $M = 1.0$. However, the increases are more near and around injection region and there is very little effect of blowing ratio downstream.

Fig. 9 presents the effect of blowing ratio on film effectiveness distributions for Case 3 (45°). For this case, the blowing ratio effect is more significant than for Cases 1 and 2. The lower blowing ratio of 0.5 is clearly the highest effectiveness. Effectiveness decreases with increasing blowing ratio. The effectiveness is almost up to 0.25 far downstream of injection for $M = 0.5$ and 1.0. Jet lift-off at $M = 1.5$ may be causing less interaction between mainstream and the jets resulting in low film effectiveness downstream around the curved surface.

Fig. 10 presents the effect of blowing ratio on Frossling number distributions for Case 3 (45°). Heat transfer coefficients are slightly higher at $M = 1.0$. The presence of attached jets at lower blowing ratio leads to enhanced heat transfer coefficients at $M = 0.5$ and 1.0 compared to $M = 1.5$. It appears that the strong compound angle can produce local mixing variations compared to smaller compound angle or baseline cases.

Fig. 11 presents the effect of blowing ratio on film effectiveness distributions for the shaped hole Case 4 (30°). The two peaks of high effectiveness are broader due to stronger diffusion of the film due to hole shaping along the leading edge surface. The film effectiveness downstream of second row with the additional compound angle is significantly enhanced compared to the baseline case. The effect is even more significant at $M = 1.0$ and 1.5 farther downstream of injection where the film effectiveness is around 0.2 compared to 0.1 for Case 1. It appears that the increase in

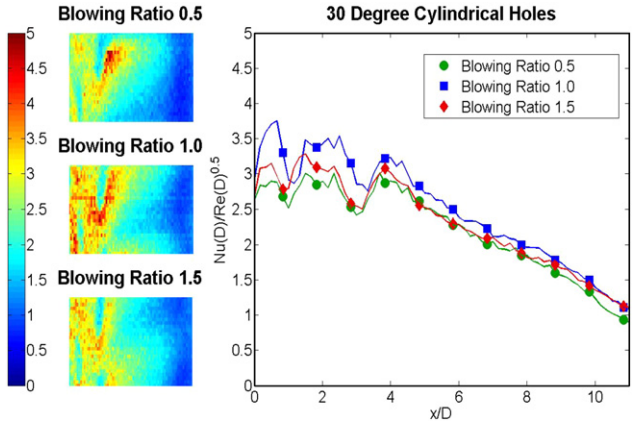

Fig. 8. Effect of blowing ratio on Frossling number distributions for Case 2.

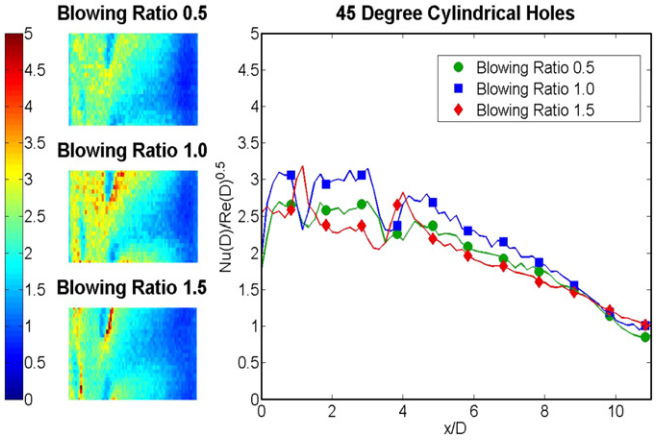

Fig. 10. Effect of blowing ratio on Frossling number distributions for Case 3.

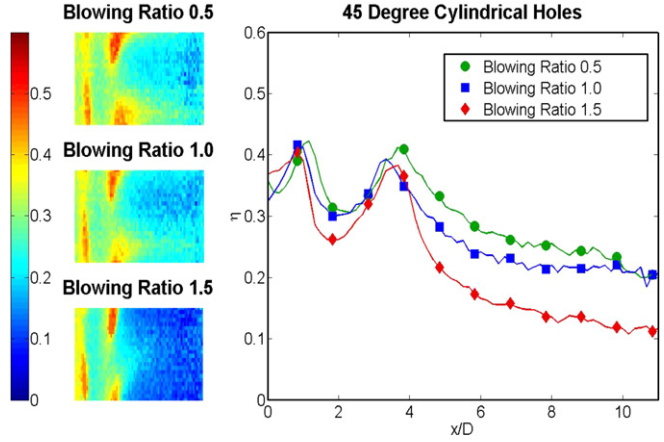

Fig. 9. Effect of blowing ratio on film effectiveness distributions for Case 3.

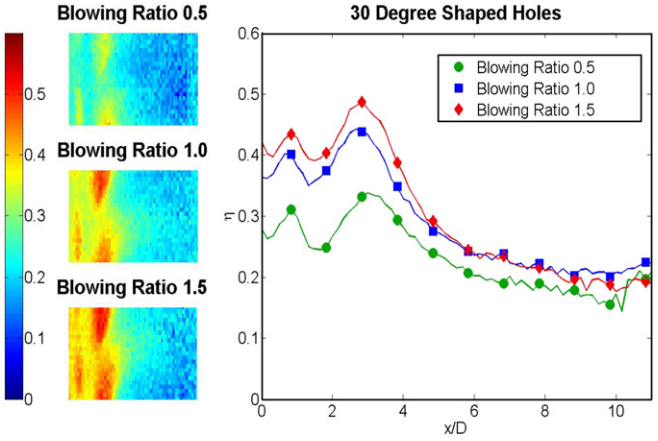

Fig. 11. Effect of blowing ratio on film effectiveness distributions for Case 4.

blowing ratio from 1.0 to 1.5 produces only a small benefit compared to increase from 0.5 to 1.0.

Fig. 12 presents the effect of blowing ratio on Frossling number distributions for Case 4 (30°). The detailed distributions show immediate high enhancement downstream of injection. In this case, it appears that heat transfer is enhanced for an increase in blowing ratio from 0.5 to 1.0. However, the increases are more near and around injection region and there is very little effect of blowing ratio downstream.

Fig. 13 presents the effect of blowing ratio on film effectiveness distributions for Case 5 (45°). For this case, the film effectiveness after the second row is significantly higher than for Cases 1–4. Effectiveness increases with increasing blowing ratio. The effectiveness is almost up to 0.25 far downstream of injection for $M = 0.5$ and 1.0. There is no indication of jet lift-off at higher blowing ratios.

Fig. 14 presents the effect of blowing ratio on Frossling number distributions for Case 5 (45°). Heat transfer coefficients are slightly higher at $M = 1.5$. The presence of attached jets at lower blowing ratio leads to enhanced heat transfer coefficients at all blowing ratios with increasing blowing ratio.

4.2. Effect of hole geometry

Fig. 15a presents the effect of hole geometry on film effectiveness distributions for $M = 0.5$. Results clearly show the benefit of adding the third compound angle and shaping the second rows of film cooling. The highest effectiveness is clearly for the shaped hole with a transverse angle of 45°. The second peak shifts downstream with the increased compound angle creating a slightly lower effectiveness area between the two rows. However, this decrease in effectiveness in the region between the holes is clearly compensated by the significant gains downstream. There is almost a 400% increase in effectiveness in region $3 < x/D < 10$ and a more than 100% increase far downstream. The further shaping of the hole exit with the additional

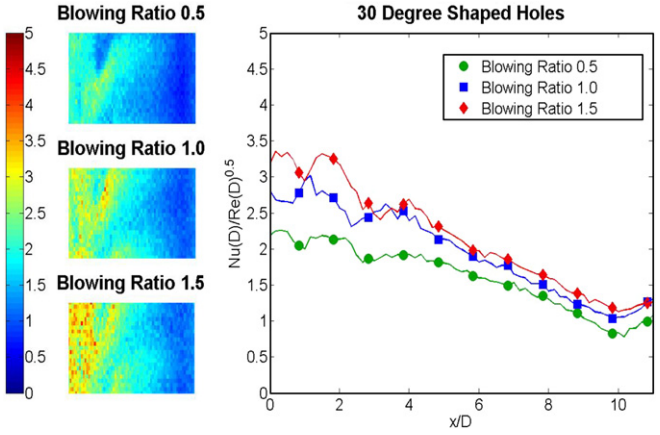

Fig. 12. Effect of blowing ratio on Frossling number distributions for Case 4.

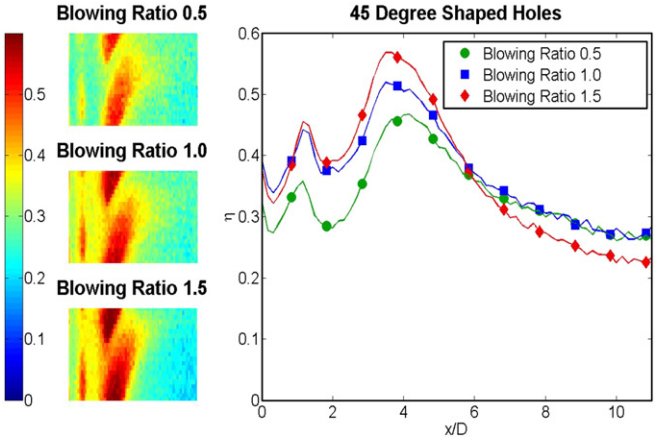

Fig. 13. Effect of blowing ratio on film effectiveness distributions for Case 5.

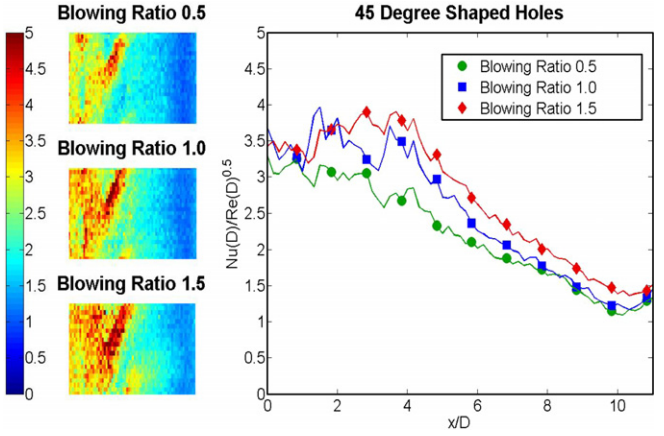

Fig. 14. Effect of blowing ratio on Frossling number distributions for Case 5.

compound angle clearly improves the overall effectiveness of the coolant film. The flat surface behind the half cylinder starts at $x/D = 11$. Beyond this point, the effect of blowing ratio is negligible.

Fig. 15b presents the effect of hole geometry on film effectiveness distributions for $M = 1.0$. At this blowing ratio, all the other geometries are relatively close to each other farther downstream but the shaped hole with compound angle of 45° is significantly superior in performance. It appears that once blowing ratio increases, a stronger compound angle is not sufficient to produce significant increases and hence shaping the exit reduces lateral momentum and thus spreading the jets on the surface.

Fig. 15c presents the effect of hole geometry on film effectiveness distributions for $M = 1.5$. The baseline case clearly outperforms the compound angle cases for this higher blowing ratio. It appears that the lift-off phenomena is causing jets to detach from the curved surface when injected through the compound angled holes resulting in lower film effectiveness both near and downstream. This result is interesting as it indicates that the baseline case

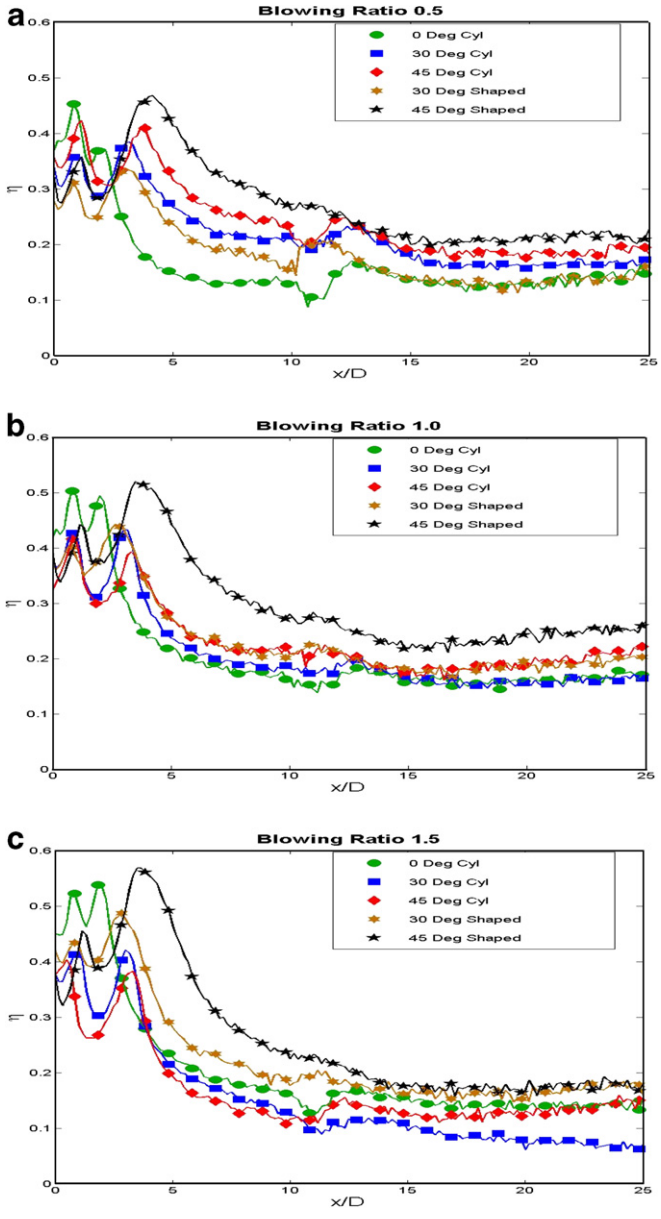

Fig. 15. Effect of hole geometry on film effectiveness distributions.

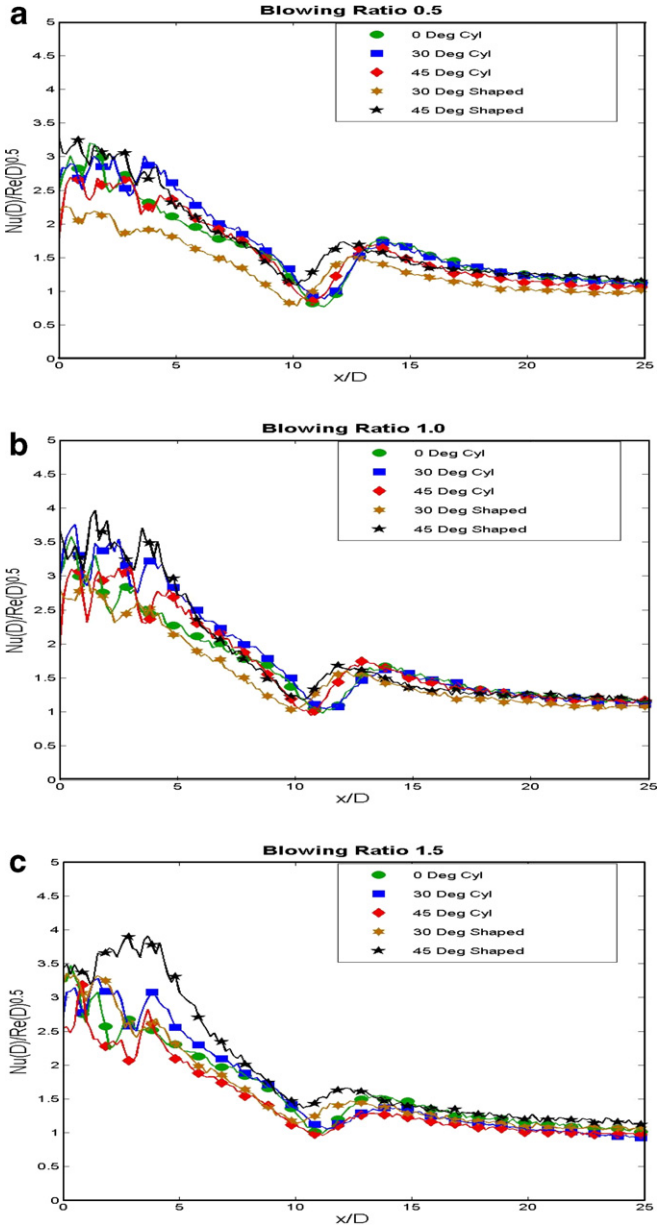

Fig. 16. Effect of hole geometry on Frossling number distributions.

keeps the coolant adhered to the surface as the injection holes are more closely packed. However, the exit shaping of the compound angle holes helps to reduce this jet lift-off and decrease the lateral momentum and thus significantly enhance film effectiveness over the baseline case. It appears that hole shaping is also beneficial at higher blowing ratios compared to just adding the compound angle.

Fig. 16 presents the effect of hole geometry on Frossling number distributions for all blowing ratios. It appears that the hole angle effect is negligible except in the region immediately downstream of the compound angle hole row where 30° angle with shaped exit produces slightly lower heat transfer coefficients. It appears that the boundary layer undergoes transition around $x/D = 10$ as a sudden increase in heat transfer is seen downstream of that point. The heat transfer coefficient continues to increase until $x/D = 15$ where transition to turbulent boundary is complete and heat transfer coefficient begins to decrease downstream.

Fig. 16b presents the effect of hole geometry on Frossling number distributions for $M = 1.0$. The results are similar to that for $M = 0.5$. Again, boundary layer transition effects are seen between x/D of 10 and 15. Although, the transition region appears to be smaller for Case 2 compared to Case 1.

Fig. 16c presents the effect of hole geometry on Frossling number distributions for $M = 1.5$. The results are similar to that for $M = 0.5$. It appears that the 45° angle hole with shaped exit produces overall higher heat transfer coefficient as expected with the higher effectiveness. However, the heat transfer increases are not significant compared to the advantages of the higher cooling effectiveness

obtained. The attached jets for shaped holes lead to local turbulence increases directly impacting heat transfer coefficients and also seem to produce a stronger boundary layer transition downstream.

Fig. 17 presents the overall averaged film effectiveness, Frossling number, and heat flux ratio distributions. The entire measured region was averaged to obtain a single value. It is interesting to note that the baseline case shows a monotonous increase in effectiveness as blowing ratio increases. Both Cases 2–3 are higher than baseline at $M = 0.5$ but decrease with increasing blowing ratio to values below baseline at $M = 1.5$. The shaped holes show a peak at $M = 1.0$ and decrease at higher blowing ratios although the values are still higher than the baseline case for Case 5 (shaped 45°). The Frossling numbers are almost similar for Cases 1–3 but Case 4 shows lower overall averaged Frossling number at lower blowing ratios. Case 5 shows the highest values due to increased mixing as explained earlier.

Fig. 18 presents the effect of blowing ratio on overall area-averaged heat flux ratio (q''/q''_0) for all five cases. This ratio indicates the reduction in heat flux obtained by introduction of film cooling over the surface. If the value is below 1.0, the effect is positive. If the value is greater than 1.0, then the presence of film cooling is detrimental. The heat flux ratio is calculated based on the formulation presented by Ekkad et al. (1997). The overall averaged heat transfer coefficient without film holes (h_0) was estimated

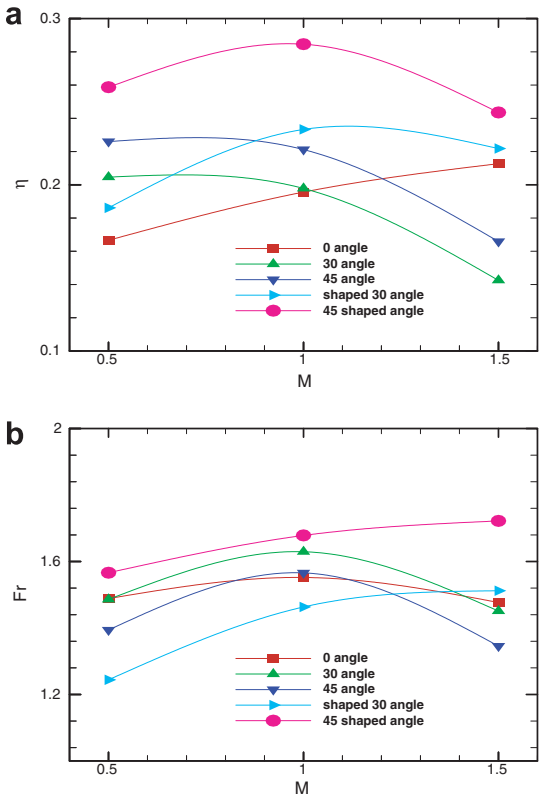

Fig. 17. Comparison of overall averaged distributions

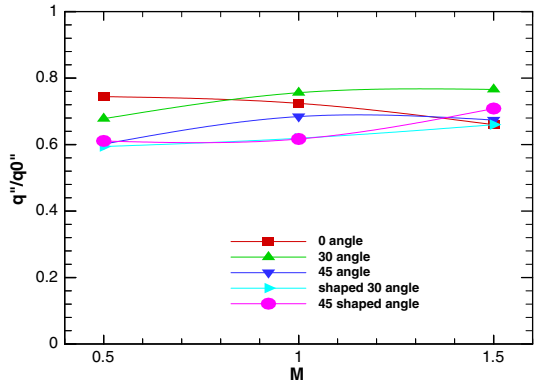

Fig. 18. Comparison of overall averaged computed heat flux ratio distributions.

based on the correlations presented by Mehendale and Han (1992). The heat transfer ratio with and without film injection (h/h_0) and the local film effectiveness are used to calculate the local heat flux ratio.

$$\frac{q''}{q''_0} = \frac{h}{h_0}\left(1 - \frac{\eta}{\phi}\right)$$

The term ϕ is the overall cooling effectiveness and ranges between 0.5 and 0.7 for typical blade cooling systems. In this study, a typical value of 0.6 is chosen. It is clear that the shaped hole cases perform very well at low blowing ratios compared to other geometries. However, the baseline case performs as well as the shaped hole cases for $M = 1.5$.

5. Conclusions

A detailed study on the effect of an additional compound angle and hole shaping on leading edge rows adjacent to stagnation row was studied. The film cooling hole angles were varied from no additional angle to 30–45°. Results show that the addition of the third compound angle on these rows increases film effectiveness significantly at lower blowing rations with increases up to 200% in certain regions. The additional compound angle induces jet lift-off at higher blowing ratios resulting in lower film effectiveness for the compound angle holes. Overall, the film effectiveness distributions are significantly altered by adding the third compound angle especially at lower blowing ratios. The heat transfer coefficient is very slightly affected by introducing this additional angle which is a positive result. Shaping the hole exit for the compounded angle significantly enhances film effectiveness over the baseline and the unshaped compound angle holes. Effectiveness enhancements are up to 150% over baseline. However, heat transfer coefficients are unaffected at lower blowing rations and although some enhancement is seen at higher blowing ratios for shaped holes. The study proves that higher cooling effectiveness can be obtained by designing more complex holes for film cooling especially in critical regions such as turbine blade leading edge region.

Acknowledgements

The authors would like to thank the NASA-LaSPACE consortium for student support through the undergraduate fellowships. The authors would like to thank Kevin Naquin, the second undergraduate student working on CFD simulations for his help with this paper.

References

Bunker, R.S., 2005. A review of shaped hole turbine film-cooling technology. ASME Journal of Heat Transfer 127, 441–453.

Cruse, M.W., Yuki, U.M., Bogard, D.G., 1997. Investigation of various parametric influences on leading edge film cooling. ASME Paper 97-GT-296.

Ekkad, S.V., Zapata, D., Han, J.C., 1997. Heat transfer coefficients over a flat surface with air and CO_2 injection through compound angle holes using a transient liquid crystal image method. ASME Journal of Turbomachinery 119 (3), 580–586.

Ekkad, S.V., Han, J.C., Du, H., 1998. Detailed film cooling measurements on a cylindrical leading edge model: effect of free-stream turbulence and coolant density. ASME Journal of Turbomachinery 120, 799–807.F.

Ekkad, S.V., Ou, S., Rivir, R.B., 2004. A transient infrared thermogrpahy method for simultaneous film cooling effectiveness and heat transfer coefficient measurements from a single test. ASME Journal of Turbomachinery 126, 597–603.

Funazaki, K., Yokota, M., Yamawaki, S., 1997. The effect of periodic wake passing on film effectiveness of discrete cooling holes around the leading edge of a blunt body. ASME Journal of Turbomachinery 119, 292–301.

Gartshore, I., Salcudean, M., McLean, I., Zhang, K., 1994. An experimental study of film cooling effectiveness near the leading edge of a turbine blade. ASME Journal of Turbomachinery 116, 71–79.

Han, J.C., Dutta, S., Ekkad, S.V., 2000. Gas Turbine Heat Transfer and Cooling Technology. Taylor and Francis, New York, NY.

Karni, J., Goldstein, R.J., 1989, Surface injection effect on mass transfer from a cylindrical in crossflow: a simulation of film cooling in the leading edge region of a turbine blade, ASME Paper No. 89-GT-276.

Kline, S.J., McClintock, F.A., 1953. Describing uncertainties in single sample experiments. Mechanical Engineering 75, 3–8.

Mehendale, A.B., Han, J.C., 1992. Influence of high mainstream turbulence on leading edge film cooling heat transfer. ASME Journal of Turbomachinery 114, 707–715.

Mick, W.J., Mayle, R.E., 1988. Stagnation film cooling and heat transfer, Including its effect within the hole pattern. ASME Journal of Turbomachinery 110, 66–72.

Mouzon, B.D., Terrell, E.J., Albert, J.E., Bogard, D.G., 2005. Net heat flux reduction and overall effectiveness for a turbine blade leading edge. ASME Paper GT2005-69002.

Ou, S., Rivir, R.B., 2001. Leading edge film cooling heat transfer with high free-stream turbulence using a transient liquid crystal image method. International Journal of Heat and Fluid Flow 22, 614–623.

Ou, S., Mehendale, A.B., Han, J.C., 1992. Influence of high mainstream turbulence on leading edge film cooling heat transfer: effect of film hole row location. ASME Journal of Turbomachinery 114, 716–723.

Reiss, H., Bolcs, A., 2000. Experimental study of a showerhead cooling on a circular cylinder comparing several configurations using cylindrical and shaped holes. ASME Journal of Turbomachinery 122, 161–169.

Vedula, R.P., Metzger, D.E., 1991. A method for the simultaneous determination of local effectiveness and heat transfer distributions in a three temperature convective situations. ASME Paper 91-GT-345.

York, W.D., Leylek, J.H., 2002a. Leading-edge film-cooling physics: Part I – adiabatic effectiveness. ASME Paper GT-2002-30166.

York, W.D., Leylek, J.H., 2002b. Leading-edge film-cooling physics: Part II – heat transfer coefficient. ASME Paper GT-2002-30167.